Supporting Information for
Oscillating Magnetoresistance in Graphene p-n Junctions at Intermediate Magnetic Felds

Hiske Overweg,[1] Hannah Eggimann,[1] Ming-Hao Liu,[2,3] Anastasia Varlet,[1] Marius Eich,[1] Pauline Simonet,[1] Yongjin Lee,[1] Kenji Watanabe,[4] Takashi Taniguchi,[4] Klaus Richter,[2] Vladimir I. Fal'ko,[5] Klaus Ensslin,[1] and Thomas Ihn[1]

[1]*Solid State Physics Laboratory, ETH Zürich, CH-8093 Zürich, Switzerland**
[2]*Institut für Theoretische Physik, Universität Regensburg, D-93040 Regensburg, Germany*
[3]*Department of Physics, National Cheng Kung University, Tainan 70101, Taiwan*
[4]*National Institute for Material Science, 1-1 Namiki, Tsukuba 305-0044, Japan*
[5]*National Graphene Institute, University of Manchester, Manchester M13 9PL, UK*

TIGHT BINDING SIMULATIONS

Overview

In the main text, we have shown a transmission map as a function of left and right carrier density, calculated using the real-space Green's function method based on the scalable tight-binding model [1]. The considered graphene ribbon of width $W = 1\,\mu$m is subject to a model density function describing an ideal *pn* junction with smoothness 50 nm. The full map is repeated here in Fig. S1(a), with a white box marking the region plotted in Fig. S1(b).

In this Supporting Information, we show more numerical results in order to demonstrate that the observed oscillation is independent of the smoothness of the *pn* junction and the width of the graphene ribbon, and is not related the current along the *pn* junction. Instead, the oscillation is shown by the last numerical test to be closely related to the Landau levels away from the *pn* junction.

For quantitative and systematic comparisons, we will focus on the density range shown in Fig. S1(b) and the line cut on it along the dashed line shown in Fig. S1(c). All calculations shown in the following consider the same density range and resolution as Figs. S1(b) and (c), which can be regarded as the reference panels of this Supporting Information. In particular, the line cut of Fig. S1(c) will be repeatedly shown in the following results.

Smoothness dependence

Figure S2(a) presents the transmission map with smoothness of 25 nm, showing a similar pattern seen in Fig. S1(b) where the junction smoothness is 50 nm. A more quantitative comparison is shown in Fig. S2(b) for the line cuts of the two cases. Despite a slightly higher T obtained for the sharper junction due to the Klein collimation [2], i.e., the sharper the *pn* junction, the wider the finite transmission probability of the angle distribution and hence the conductance, the general trend of the oscillation is shown to be independent of the smoothness.

In the rest of the numerical results, the smoothness will be fixed to 50 nm.

Width dependence

Figure S3 presents the transmission map based on a graphene ribbon with $W = 0.9\,\mu$m shown in its panel (a) and $W = 0.8\,\mu$m shown in its panel (b). Comparing the line cuts in Fig. S3(c), along with the reference line of Fig. S1(c) for the case of $W = 1\,\mu$m, the feature of the oscillation is clearly shown to be width-independent. On the other hand, the oscillation amplitude decreasing with the reduced graphene width implies that the oscillation may be closely related to the Landau levels in the bulk away from the *pn* junction, since the wider the graphene ribbon the better the Landau levels can develop.

In the rest of the numerical results, the graphene width will be fixed as $W = 1\,\mu$m.

Strong lattice defects

Next we show that the oscillation is not related to the current along the *pn* junction. To this end, we consider large-area lattice defects located in the vicinity of the *pn* junction. The basic idea is that if the oscillation came from any interference due to the current along the *pn* junction, such as the snake state [3], a large-area lattice defect at the *pn* interface or in the vicinity of it would act as a strong scatterer, destroying the

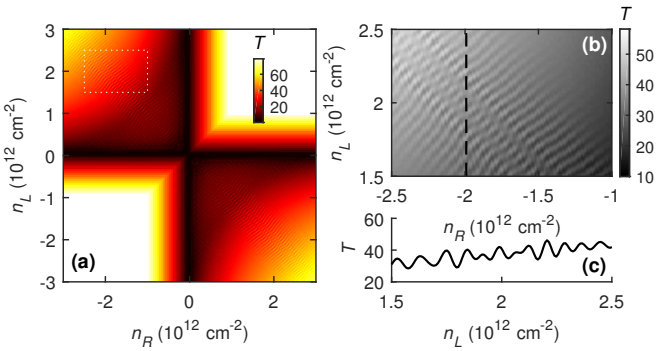

FIG. S1. (a) Transmission map $T(n_R, n_L)$ same as Fig. 5(a) in the main text (smoothness 50 nm and graphene width $W = 1\,\mu$m); white dashed box marks the region shown in (b), where a black dashed line indicates the line cut of $T(n_L)$ at fixed $n_R \approx -2 \times 10^{12}\,\mathrm{cm}^{-2}$ shown in (c).

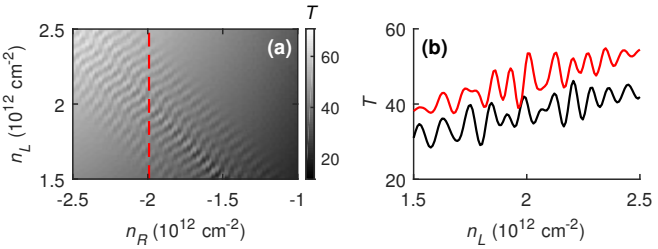

FIG. S2. (a) Transmission map $T(n_R,n_L)$ similar to Fig. S1(b) but with smoothness 25 nm of the *pn* junction. The red dashed line indicates the line cut shown as a red line in (b), where the black line is the reference line identical to Fig. S1(c) for the case with smoothness 50 nm.

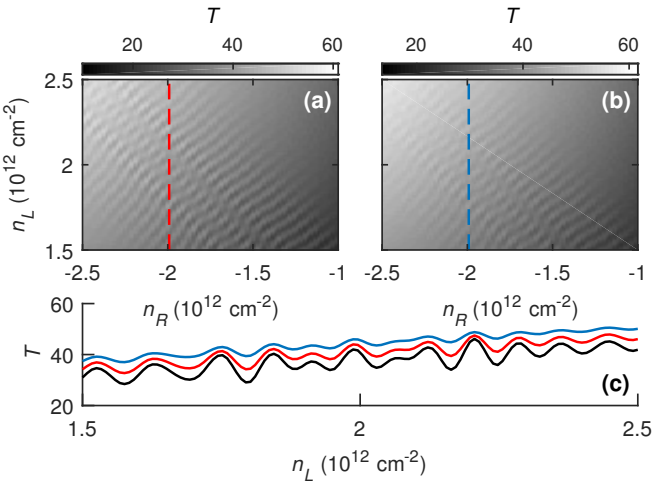

FIG. S3. Transmission maps $T(n_R,n_L)$ similar to Fig. S1(b) with the same smoothness of 50 nm but with (a) $W = 0.9\,\mu$m and (b) $W = 0.8\,\mu$m. Line cuts along the red/blue dashed line marked in (a)/(b) are compared in (c) together with the reference line (black) of Fig. S1(c) for the case of $W = 1\,\mu$m.

interference and hence suppressing the oscillation. Contrarily, if the oscillation survives the introduced large defects, the current along the *pn* junction will then be ruled out from possible origins of the oscillation.

We first consider a $50 \times 400\,\text{nm}^2$ defect in Figs. S4(a) and (b); the defect is placed in front of the *pn* junction (at a distance 150 nm) in the former, and exactly on the *pn* junction in the latter. Despite an additional modulating pattern observed in Fig. S4(a), the fine oscillation patterns remain visible in both cases. By increasing the defect area to $300 \times 300\,\text{nm}^2$, the transmission map shown in Fig. S4(c) still exhibits the same oscillation pattern. A quantitative comparison of the line cuts summarized in Fig. S4(d) together with the reference line from Fig. S1(c) clearly shows that the oscillations observed in Figs. S4(a)–(c) belong to the same type as all those shown previously.

The fact that the strong defect introduced in the vicinity of the *pn* junction cannot suppress the oscillation clearly indicates that any possible interference effect due to the current

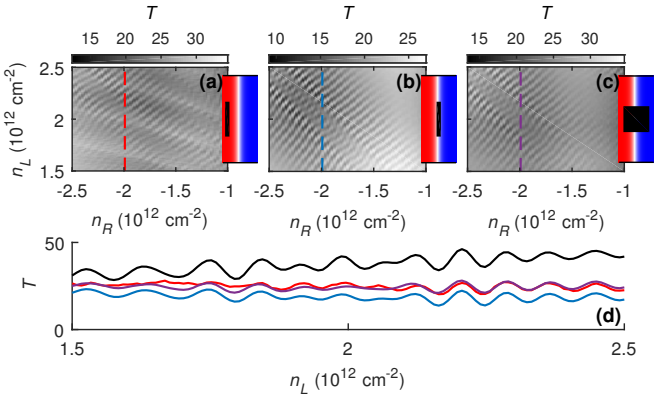

FIG. S4. (a)–(c) Transmission maps $T(n_R,n_L)$ similar to Fig. S1(b) with the same smoothness of 50 nm and width $W = 1\,\mu$m, but with a large-area defect represented by the black rectangle shown in the individual inset to the right of each panel, where the color background depicts the y-independent model function $n(x,y)$ describing the density variation of the *pn* junction. The size of the defect is $50 \times 400\,\text{nm}^2$ in (a,b) and $300 \times 300\,\text{nm}^2$ in (c). Line cuts along the red/blue/purple dashed line marked in (a)/(b)/(c) are compared in (d) together with the reference line (black) of Fig. S1(c) for the case without the defect.

along the *pn* junction cannot be the origin causing the oscillation. Instead, the oscillation seems to depend only on the Landau levels that are well developed in the semi-infinite leads.

Fixed leads

So far, all the presented calculations are based on an infinite graphene ribbon with a *pn* junction in the middle, as described in the main text. Technically, this is achieved in numerics by considering a scattering region of size $L \times W$ attached to two leads from the left and right, both floating with the density profiles at the attaching edge of the scattering region. As long as L is much longer than the smoothness of *pn* junction ($L =$ 400 nm has been adopted in all the presented calculations), the density values at the left and right edges of the scattering region will saturate to a constant, and the entire open quantum system of the finite-size scattering region attached to the two floating semi-infinite leads will resemble an ideal *pn* junction in the middle of an infinitely long graphene ribbon, exhibiting an L-independent transmission behavior.

As a final and conclusive numerical test, we now fix the Fermi energies in the two semi-infinite leads at 0.1 eV, and consider the same range and parameters as the reference panel of Fig. S1(b). The calculated transmission map is shown in Fig. S5(a), which no longer exhibits the fine oscillation. The line cuts of fixed leads vs. floating leads compared in Fig. S5(b) clearly show that the oscillation completely vanishes in the present case of fixed leads.

The vanishing oscillation is consistent with what we have speculated from the previously shown tests that the oscillation originates from the resonance between Landau levels well de-

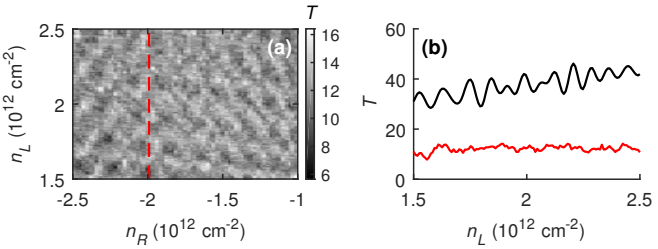

FIG. S5. (a) Transmission map $T(n_R, n_L)$ with the same range and parameters considered in Fig. S1(b) but with the two leads fixed at energy $E = 0.1\,\mathrm{eV}$. The red dashed line indicates the line cut shown as a red line in (b), where the black line is the reference line identical to Fig. S1(c) for the case with floating leads.

veloped in the far left and far right in the semi-infinite leads. The present case shown in Fig. S5 considers fixed Fermi energies in the leads that no longer float with the densities n_R and n_L. Together with the fact that the length $L = 400\,\mathrm{nm} \ll W$ of the scattering region is too short for the Landau levels to form, the vanishing oscillation is therefore reasonably expected. By increasing the length of the scattering region to at least $L \approx W$, revival of the oscillation is expected for the case of fixed leads.

Note that the situation of fixed leads is actually closer to the experiment, because the densities in graphene regions close to the contacts are rather pinned by the contact doping. However, the samples in our experiments (summarized in Table I in the main text) are long enough (several microns in all samples) for the Landau levels to develop well (with level spacing not far enough compared to disorder broadening in the magnetic field range we focus on) due to their cleanness and therefore exhibit the oscillation. Our numerical results based on floating leads correspond to the ideal case of infinitely long samples and therefore exhibit optimized oscillation.

MAGNETORESISTANCE OSCILLATIONS IN SAMPLES B-F

Figures S6-S10 show magnetoresistance oscillations of samples B-F, which look similar to the ones observed in sample A (see Fig. 3 of main text). The periodicity of the oscillations is the same for all samples.

4-terminal measurements in sample D

The device layout of sample D is schematically shown in Fig. S11. A DC voltage of $100mV$ was applied to the sample with a $R = 10\ \mathrm{M\Omega}$ resistor in series. This led to a constant current of $I = 10$ nA flowing from contact 1 to contact 4. The voltage drop between contact pairs (1,2), (2,3) and (3,4) where measured. To calculate the conductance a contact resistance was subtracted where appropriate. As is shown in Fig. S11b-d, the oscillatory magnetoresistance is only observed when a p-n interface is present (i.e. in between contacts (2,3)).

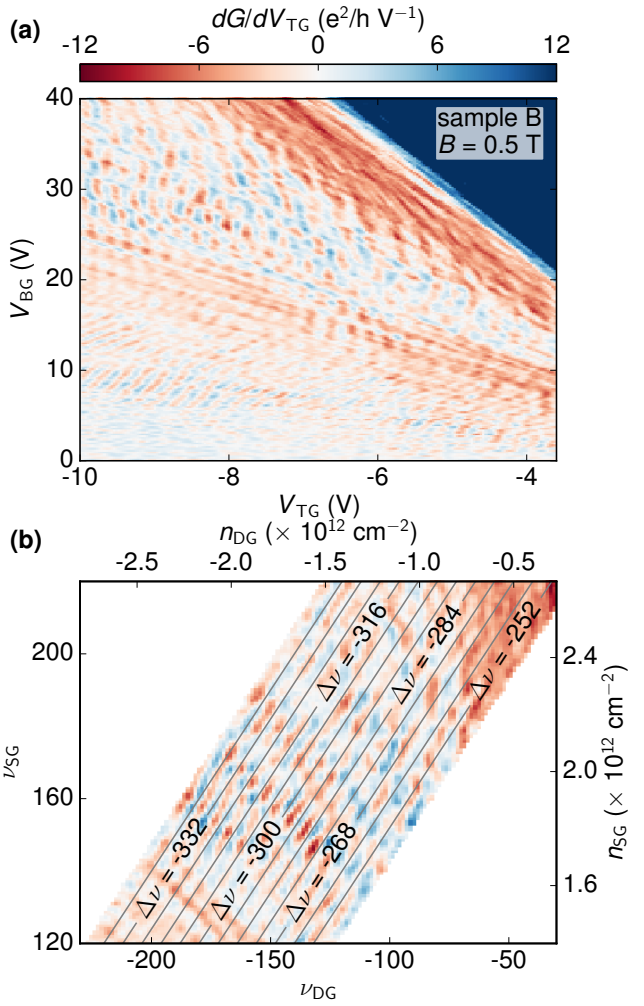

FIG. S6. (a) Transconductance dG/dV_{TG} of sample B at $B = 0.5$ T. (b) Transconductance as a function of filling factor in the single and double gated region.

* overwegh@phys.ethz.ch

[1] M.-H. Liu, P. Rickhaus, P. Makk, E. Tóvári, R. Maurand, F. Tkatschenko, M. Weiss, C. Schönenberger, and K. Richter, Phys. Rev. Lett. **114**, 036601 (2015).
[2] V. V. Cheianov and V. I. Fal'ko, Phys. Rev. B **74**, 041403 (2006).
[3] P. Rickhaus, P. Makk, M.-H. Liu, E. Tóvári, M. Weiss, R. Maurand, K. Richter, and C. Schönenberger, Nat. Commun. **6**, 6470 (2015).

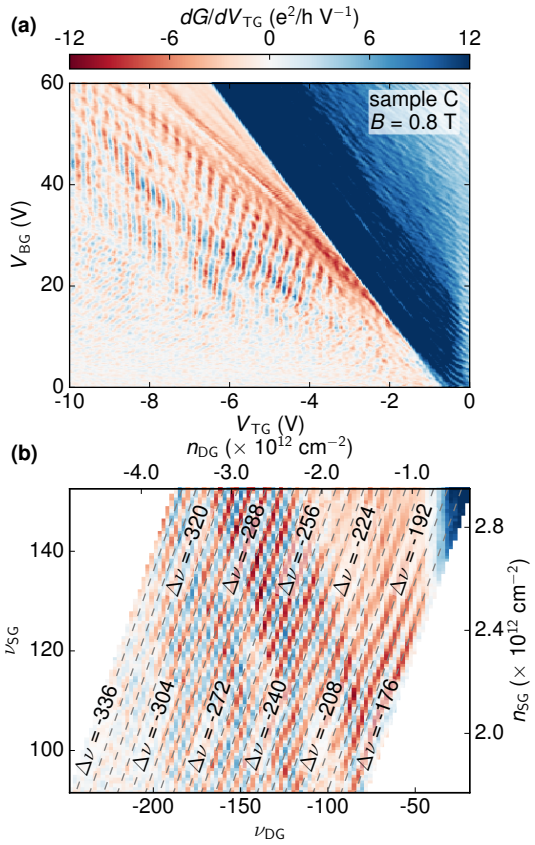

FIG. S7. a) Transconductance dG/dV_{TG} of sample C at $B = 0.8$ T. (b) Transconductance as a function of filling factor in the single and double gated region.

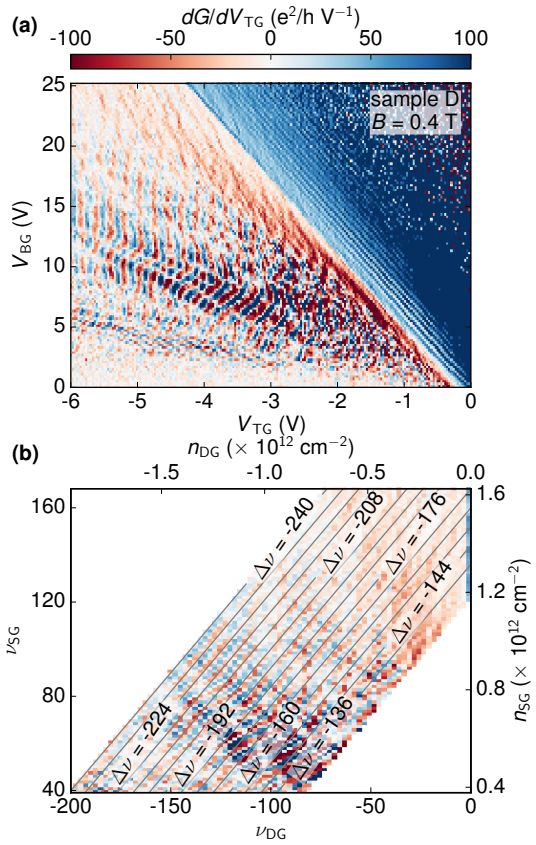

FIG. S8. (a) Transconductance dG/dV_{TG} of sample D at $B = 0.4$ T. (b) Transconductance as a function of filling factor in the single and double gated region.

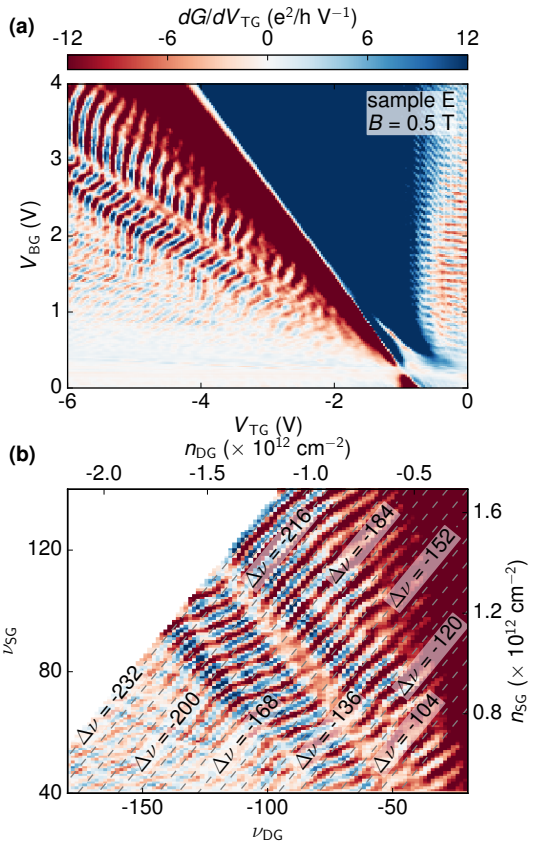

FIG. S9. (a) Transconductance dG/dV_{TG} of sample E at $B =$ 0.5 T. (b) Transconductance as a function of filling factor in the single and double gated region.

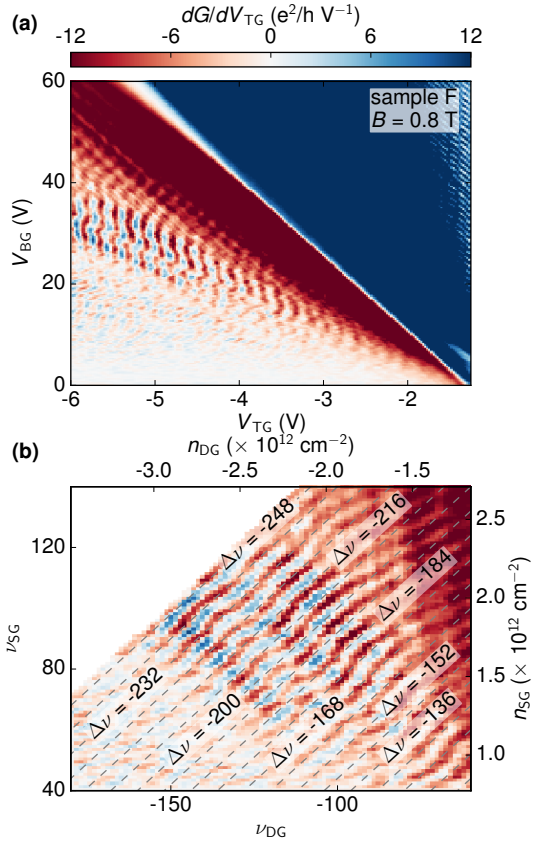

FIG. S10. (a) Transconductance dG/dV_{TG} of sample F at $B =$ 0.8 T. (b) Transconductance as a function of filling factor in the single and double gated region.

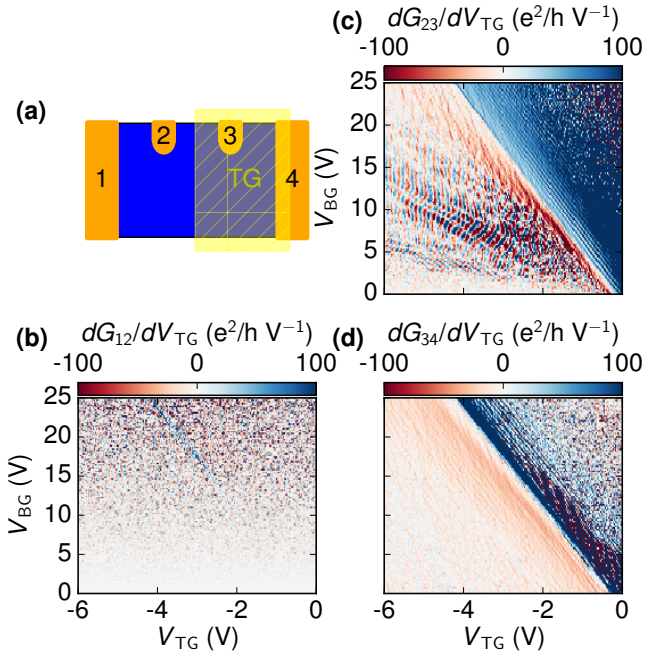

FIG. S11. (a) Schematic drawing of sample D. Contacts are labelled 1-4. (b) Transconductance between contacts (1,2) at $B = 0.4$ T. (c) Transconductance between contacts (2,3) showing an oscillatory pattern in the *p*-*n* regime. (d) Transconductance between contacts (3,4).